nature plants

ARTICLES

https://doi.org/10.1038/s41477-020-0602-x

Advanced vascular function discovered in a widespread moss

T. J. Brodribb[1]✉, M. Carriquí[1,2], S. Delzon[3], S. A. M. McAdam[4] and N. M. Holbrook[5]✉

The evolution of terrestrial plants capable of growing upwards into the dry atmosphere profoundly transformed the Earth. A transition from small, 'non-vascular' bryophytes to arborescent vascular plants during the Devonian period is partially attributed to the evolutionary innovation of an internal vascular system capable of functioning under the substantial water tension associated with vascular water transport. Here, we show that vascular function in one of the most widespread living bryophytes (*Polytrichum commune*) exhibits strong functional parallels with the vascular systems of higher plants. These parallels include vascular conduits in *Polytrichum* that resist buckling while transporting water under tension, and leaves capable of regulating transpiration, permitting photosynthetic gas exchange without cavitation inside the vascular system. The advanced vascular function discovered in this tallest bryophyte family contrasts with the highly inefficient water use found in their leaves, emphasizing the importance of stomatal evolution enabling photosynthesis far above the soil surface.

Fossils of the earliest vascular plants indicate that they were small in stature and, similar to extant bryophytes, restricted to growing within the diffusion boundary layer near the soil where high humidity and CO_2 enable photosynthesis with minimal desiccation[1–4]. The capacity to elevate photosynthetic tissue aloft in a dry atmosphere evolved during the Devonian period, leading to the formation of the first forests[5] and the transformation of terrestrial Earth. Nevertheless, the key anatomical and physiological innovations that allowed vascular plants to increase in size dramatically during this period have been the subject of debate for over 150 yr[6]. The evolution of features capable of maintaining photosynthetic tissues hydrated and functional in a dry atmosphere is considered critical to explaining the success of vascular plant evolution[7,8]. These features include (1) a lignified water transport system conducting water to photosynthetic structures, (2) photosynthetic tissues encased in an impermeable cuticle and (3) adjustable stomatal valves regulating CO_2 and water vapour exchange with the atmosphere to enable photosynthesis while preventing damage by uncontrolled dehydration[8,9]. Like their common ancestor with vascular plants, the bryophytes are thought to lack these vascular plant components, confining their photosynthetic activity to moist environments close to the substrate. However, recent work shows surprising homologies between the developmental genetics of bryophytes and angiosperms[10–13], raising new questions about what prevented bryophytes from increasing in stature before, or alongside, the evolution of vascular plants.

The moss family Polytrichaceae represents an exceptional group of bryophytes, equipped with well-developed water-conducting cells (hydroids[14,15]), and includes species with the capacity to grow >300 mm in height. These qualities provide an excellent system in which to investigate the prerequisite elements necessary for the evolution of areal photosynthetic organs. Although the potential for hydroids to enhance internal water transport has long been recognized[14,16–19], they have been assumed to lack the reinforcement needed to withstand the internal (negative) pressures that drive water transport in the xylem of vascular plants[20,21]. In this study we use living specimens of *Polytrichum commune* to evaluate the classical theory that vascular plants are unique in possessing an internal hydraulic vascular system capable of delivering water under tension to photosynthetic tissues.

Results and Discussion

Resistance to buckling. Vascular plants use the combination of hollow dead cells and a substantial water potential gradient to move the large fluxes of water required for canopy photosynthesis and leaf temperature regulation. This transport mechanism requires incorporation of the high-density polyphenolic compound, lignin, into the walls of water-transporting xylem cells to prevent the collapse of conduits when exposed to hoop stress produced by housing water under tension (negative water potentials)[22]. It is widely believed that only vascular plants evolved a lignified water transport system[23,24,] meaning that bryophytes should be incapable of extracting soil water and maintaining an active transpiration stream without the collapse of non-lignified transport cells. We tested this assumption using scanning electron cryomicroscopy (cryoSEM) to determine whether the hydroids of *P. commune* resist buckling when exposed to the range of tensions used by vascular plants to extract water from the soil. Hydroids were found to sustain liquid water in the lumen without buckling or deformation when exposed to water potentials as low as −1.45 megaPascals (MPa; Fig. 1). By maintaining structural integrity at water potentials within the operational range of angiosperm leaves[25], the hydroids of *Polytrichum* demonstrate the capacity to transport water under tension in a similar fashion to vascular plants. This unexpected result suggests that the hydroids of *Polytrichum* may contain some lignin[26] or a related polymer with similar mechanical stiffness. Our data call into question the long-held assumption that the evolution of lignified xylem in vascular plants was a prerequisite for internal water transport under tension.

[1]School of Natural Sciences, University of Tasmania, Hobart, Tasmania, Australia. [2]Research Group on Plant Biology under Mediterranean Conditions, Departament de Biologia, Universitat de les Illes Balears – Instituto de Investigaciones Agroambientales y de la Economía del Agua, Palma, Spain. [3]Université Bordeaux, BIOGECO, INRAE, Pessac, France. [4]Purdue Center for Plant Biology, Department of Botany and Plant Pathology, Purdue University, West Lafayette, IN, USA. [5]Department of Organismic and Evolutionary Biology, Harvard University, Cambridge, MA, USA. ✉e-mail: timothyb@utas.edu.au; holbrook@oeb.harvard.edu

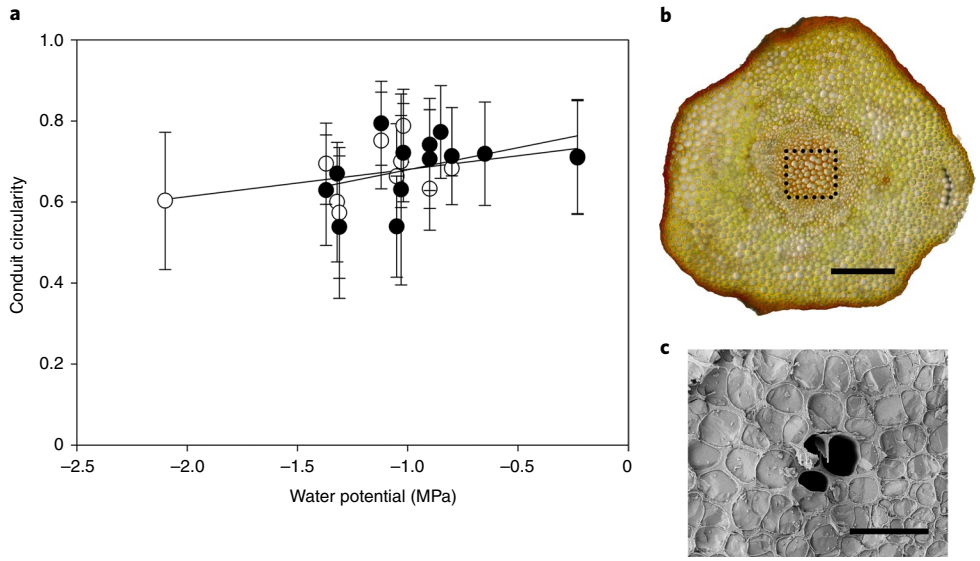

Fig. 1 | *P. commune* vascular tissue is capable of sustaining large hydraulic tension without collapsing. a, Conduit circularity was measured in the hydroids (putative water transport tissue) of 14 moss plants exposed to dehydration, which were immediately frozen in liquid nitrogen before imaging with SEM. Mean circularity (± s.d.) of water-filled conduits in each plant (one measure per plant, filled symbols) remained high across the range of water potentials, although an increasing number of air-filled conduits (open circles) were observed in more dehydrated samples. Conduit circularity was not significantly correlated with water potential for either water-filled (Pearson correlation $r = 0.42$, $P > 0.1$) or air-filled ($r = 0.46$, $P > 0.1$) conduits. Hydroid cells were sampled from the central hydrome vascular strand. **b**, Stem cross-section of the hydrome, indicated by the dotted box; scale bar, 100 µm. **c**, CryoSEM preserved cell shape under native tension, allowing air-filled hydroids (black lumina) to be distinguished from water-filled hydroids; scale bar, 20 µm.

Water transport efficiency and cavitation. Having established that *Polytrichum* hydroids have the physical capacity to transport water under tension, we measured the conductive capacity (hydraulic conductance) of the moss vascular system to determine whether water flow through hydroids could be sufficient to support photosynthesis. In vascular plants there is a general linkage between the capacity of leaves to transport water and their photosynthetic capacity[27]. Measurements of the maximum assimilation rate and internal hydraulic conductance of *P. commune* shoots indicated a ratio of water transport efficiency to photosynthetic capacity similar to that found in vascular plants (Extended Data Fig. 1). Furthermore, the almost equal distribution of conductance between below- and above-ground tissues in *P. commune* is similar to what occurs in vascular plants[28] (Extended Data Fig. 2). Thus we find that, despite the non-homologous development of water-conducting cells in *Polytrichum* compared with vascular plants[20], this moss has a fully functional vascular system capable of transporting a continuous stream of water from the soil, through hydroids and up into the leaves. Despite the fact that *Polytrichum* hydroids are imperforate, in contrast to the conduits of vascular plants[20], we found that the flow of water through the moss vascular system was sufficient to maintain stable leaf hydration and steady-state photosynthesis in an evaporating environment. This function has previously been considered the preserve of vascular plants.

In vascular plants a critical limitation on water transport is that the continuous water column contained within the non-living pipeline of tubular xylem cells becomes meta-stable when the water potential falls below the equilibrium vapour pressure[22]. Thus, plants exposed to drying soil or strong evaporative demand become increasingly vulnerable to the formation of bubble emboli in the vascular conduits (loosely termed 'cavitation'). Xylem cavitation permanently blocks water flow in affected cells, leading to tree death during drought[29,30]. Having determined that the vascular system of *Polytrichum* operates under tension, we expected that it would also be prone to embolism formation under water stress, as previously observed during freeze–thaw treatments[31]. We used three independent techniques (optical imaging, X-ray tomography and cryoSEM) to examine hydroids of *Polytrichum* during imposed water stress and thus to test whether dehydration caused cavitation in the moss vascular system. All methods indicated that hydroids could resist cavitation until water potentials fell below −0.5 MPa, at which point the onset of cavitation in the central hydroid bundle was observed. Optical visualization of cavitation showed that 50% of the vascular tissue was embolized at a mean water potential of −1.8 MPa, and this was confirmed by cryoSEM imaging (Fig. 2). High-resolution X-ray imaging also identified cavitation localized to hydroid cells once water potentials fell within the same range, between −1 and −1.9 MPa (Fig. 2b). In addition, we found that shoot hydraulic conductance fell rapidly in this same range (Extended Data Fig. 3). The observed vulnerability of *P. commune* vasculature to water stress-induced cavitation was well within the vascular plant spectrum, similar to the herbaceous leaves of sunflower[32] or tree species such as poplar or willow[33]. Similar to observations in cushion-forming vascular plants[34], rapid repair of embolized conduits was observed when *P. commune* plants were re-wetted after dehydration (Extended Data Fig. 4 and Supplementary Video 1).

Regulated gas exchange. Unlike vascular plants, many mosses, including *Polytrichum*, are desiccation tolerant, meaning that they do not need to maintain hydration to survive. The finding that *Polytrichum*, like vascular plants, relies on a continuous water column to maintain photosynthesis raises the question of how a moss, classified as poikilohydric (meaning it has no control over its water content), could benefit from a water supply system that is vulnerable to cavitation. Vascular plants use stomatal valves on the leaf surface to protect the water transport system from cavitation, by reducing transpiration before xylem cavitation is initiated during evaporative or soil water stress[32]. Dynamic regulation of transpiration is a fundamental adaptation in vascular plants that enables them to grow in environments where unregulated transpiration would lead to rapid cavitation[25]. We sought to determine whether *P. commune* showed any similar capacity to protect the integrity of the internal water

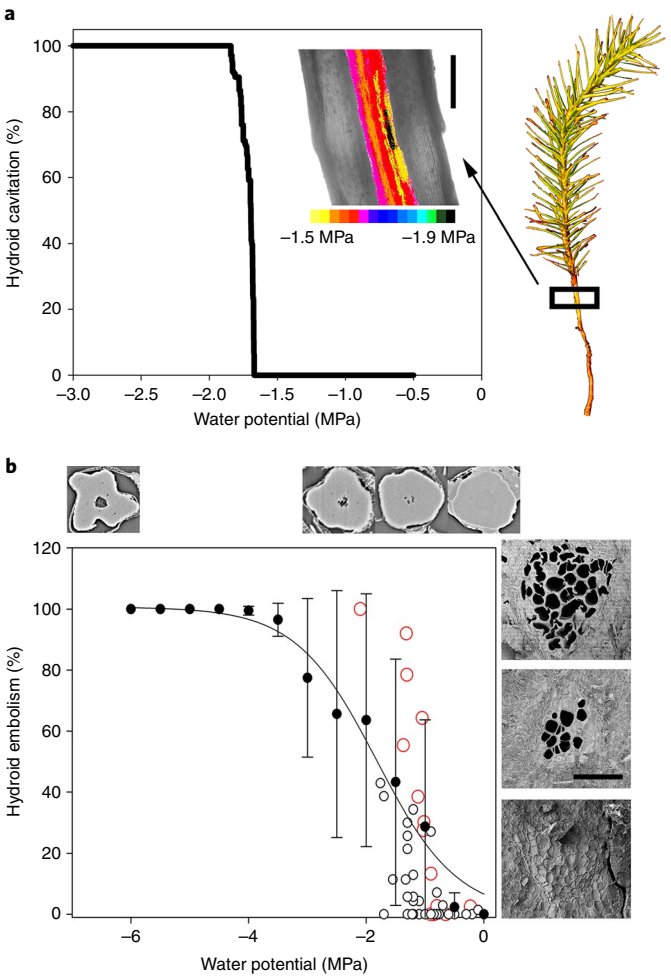

Fig. 2 | The water transport system in *P. commune* shows a pattern of vulnerability to cavitation-induced failure similar to that seen in vascular plants. a, In situ spatio-temporal mapping of cavitation, determined by rapid changes in tissue optical transmission, shows that during moisture stress the water transport system of moss resists cavitation under substantial water tension. Data from a single individual stem initially show no evidence of xylem dysfunction until a burst of cavitation occurs as water potential falls between -1.45 and -1.85 MPa. Cavitation events are localized to the central conducting tissue of the moss. Insert: coloured pixels localize individual cavitation events and are colour-coded according to the water potential when each event occurred; scale bar, 500 µm. **b**, Mean hydroid embolism (± s.d., $n = 9$ individuals) at a range of water potentials from 0 to −6 MPa shows the average vulnerability to cavitation according to optical measurements (filled circles plus least-squares regression fitted to a sigmoidal model), whereby 50% of water-transporting conduits cavitated at −1.8 MPa. Similar plots are shown using embolism counts from cryoSEM samples (open red circles) and high-resolution X-ray tomography (open black circles). Representative images from these methods are shown on the *y* (cryoSEM; scale bar, 200 µm) and *x* (micro-computed tomography field of view, 500 µm) axes, respectively. In both cases, cavitated, air-filled conduits are seen as black voids.

column by regulating transpiration to avoid cavitation. Maximum diffusive conductance to water vapour in *Polytrichum* leaves was high (equivalent to the highest values measured in angiosperms) in hydrated individuals but, remarkably, we found that leaf diffusive conductance declined to <15% of maximum values as plants dehydrated to water potentials of −1.5 MPa (Fig. 3a). The dramatic reduction in water loss before the onset of major cavitation of the vascular system observed in this moss species was highly reminiscent of the pattern seen in vascular plants where stomatal valves on the leaf surface close during dehydration, delaying the onset of cavitation damage to the vasculature[35].

Polytrichum gas exchange also responded to humidity in a fashion consistent with a regulatory process functioning to delay cavitation. Based on the measured hydraulic conductance of whole moss plants, we predicted that without regulated transpiration, hydroid cavitation would occur when atmospheric humidity fell below a very moderate 80% relative humidity at 25 °C (Fig. 3b). However, it was observed that *P. commune* plants measured in situ could maintain steady-state photosynthesis above zero down to 10% relative humidity at 22 °C (Fig. 3b). This ability of *Polytrichum* plants to function in relatively dry air was associated with dramatic and reversible reductions in whole-plant diffusive conductance (g) in response to increasing evaporative demand (Fig. 3 and Extended Data Fig. 5). The decline in g before the onset of cavitation was highly reminiscent of the pattern produced by stomatal closure in vascular plants[36], enabling *Polytrichum* to maintain steady-state photosynthesis under a wide range of humidity without incurring cavitation in the water transport system. Such dynamic control of evaporation was highly unexpected in a moss, where there are no stomatal valves on the photosynthetic surface to regulate transpiration.

Changes in the conformation of leaves at different states of hydration might explain the transpirational regulation of *P. commune* in response to water stress[37]. In hydrated plants the photosynthetic lamellae on the upper surface of leaves are separated, allowing rapid diffusion of water vapour and CO_2 between the large surface area of photosynthetic cells and the atmosphere. However, in mildly dehydrated leaves the leaf margins curl inwards causing enlarged, wax-covered 'terminal cells' on the lamellae to close together, effectively isolating the bulk of the gas exchange surface from the atmosphere[38]. In addition, declining diffusive conductance was strongly correlated with changes in leaf angle such that leaves become appressed to the stem before the onset of cavitation (Extended Data Fig. 6). Both processes are likely to limit transpiration by reducing the evaporative surface area and increasing the boundary layer, thereby limiting the loss of water and the uptake of CO_2 during photosynthesis.

Water-use efficiency. Although *P. commune* shares a form of regulatory protection of the vascular system similar to that of vascular plants (Fig. 3), a major difference we observed in the moss was an exceptionally high sensitivity of photosynthesis to changes in atmospheric humidity (Fig. 4a and Extended Data Figs. 7 and 8). The reason was revealed when we compared pooled gas exchange data from 84 species representing vascular plant clades that diverged before the evolution of seed plants (lycophytes and ferns). Despite occupying a similar range of photosynthetic output, we found that the intrinsic water-use efficiency (A/g) of these early-branching vascular plant groups is much higher than in *P. commune* (Fig. 4b and Extended Data Fig. 9). The combination of inefficient water use and the regulation of plant water potential in a non-cavitating range required moss diffusive conductance to be highly sensitive to humidity. Photosynthetic rate was affected, because reduced diffusive conductance to water vapour was apparently also linked to the diffusion of CO_2 into the photosynthetic tissue (Figs. 3b and 4b). In vascular plants, proportionality between assimilation rate and g is an expected consequence of the common diffusive limitation on the movement of water vapour and CO_2 through stomata, but unexpected in leaves without stomata such as those of *Polytrichum*. An inefficient exchange ratio between water and carbon in *Polytrichum* probably derives from the very high cellular resistance to CO_2 diffusion in its leaves. In common with other moss species[39], *Polytrichum* plants were also found to have a high diffusive conductance to water vapour even when $A = 0$ (Fig. 4b) and, as a result, are not able to delay desiccation to the same extent as stomata-bearing vascular plants.

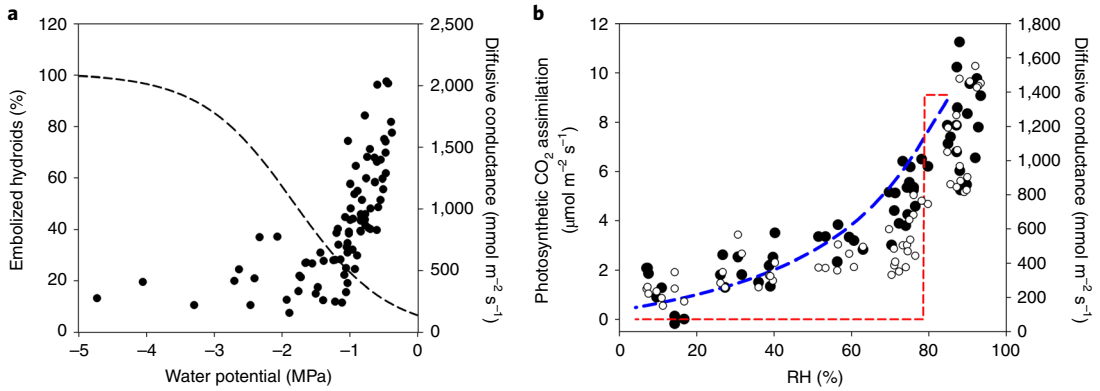

Fig. 3 | Similar to vascular plants, the leaves of *P. commune* regulate water loss during water stress to delay the onset of damaging cavitation in the water transport system. a, Black circles denote the effect of shoot dehydration on the diffusive conductance of leaves to water vapour. Declining water potential causes a sharp decrease in moss leaf vapour conductance, to a minimum value between −1 and −1.5 MPa. This minimum corresponds closely to the water potential causing incipient cavitation in the vascular system (dashed curve denotes vulnerability of the moss stem to cavitation shown in Fig. 2b). **b**, Steady-state measurements of diffusive conductance to water vapour (open circles) and photosynthetic uptake of CO_2 in the leaves (filled circles) of well-irrigated moss individuals equilibrated at a range of relative humidity (RH). Diffusive conductance and photosynthetic rate were actively restricted at lower humidity, declining in a manner that closely matched the modelled pattern of CO_2 uptake (blue dashed line) required to maintain plant water potential outside the range that would induce cavitation damage to the vascular system. The modelled effect of humidity on photosynthesis in leaves where diffusive conductance was not regulated (red dashed line) shows failure of the hydraulic system and loss of photosynthetic function at humidity close to 80%.

In combination these factors mean that, despite possessing a fully functional vascular system, the protection of this system against cavitation renders photosynthesis in *Polytrichum* highly sensitive to humidity, probably preventing it from competing with vascular plants far above the surface boundary layer. At the same time, sensitivity to humidity may also explain why *P. commune* typically grows with its below-ground organs (rhizomes and rhizoids) in standing water, preventing the development of soil water deficit and providing the moist air required for it to sustain high rates of photosynthesis. Other factors that have been considered as constraints on bryophyte stature include the dominance of a gametophyte generation that relies on externally swimming sperm for fertilization (although *Marchantia* sperm have been shown to move up to 19 m[40]), and the absence of lignified tissues capable of providing the mechanical support needed for extensive upright growth[41]. While these factors may influence bryophyte morphology and reproduction, our data focus on the physiological demands associated with elevation of photosynthesis into the air.

Conclusion

The moss *Polytrichum* thus provides clear evidence that the functional hurdles preventing 'non-vascular' plants from sustaining photosynthesis in a dry atmosphere are neither deficiencies in water transport nor the regulation of transpiration. Rather, it appears that their profoundly inefficient exchange ratio of water for photosynthetic CO_2 explains the inability of even the most hydraulically proficient moss species to emerge far from the surface boundary layer and achieve positive carbon gain in a turbulent and dry atmosphere. Our research reveals that *Polytrichum* possesses an efficient vascular system that is functionally comparable to that of vascular plants. This parallel extends to the regulation of transpiration to protect moss vascular tissues from cavitation, a feature of stomatal control in vascular plants. These data provide a functional context for recent studies pointing to genetic homology in the vascular developmental pathways used by bryophytes and vascular plants[11]. We propose that vascular plant innovations associated with improvement in water use efficiency, such as cuticle formation, the location of stomata on photosynthetic surfaces and high mesophyll conductance to CO_2, are more fundamental to the evolution of vascular plants than the vascular system from which they derive their name.

Methods

Plant material. *Polytrichum commune* plants were collected from a single population growing on Mt. Wellington in Tasmania (42.92° S, 147.26° E). Several large slabs containing >500 individual shoots were removed with soil, without damaging the plants, and transferred to a misting glasshouse where plants were maintained under a natural photoperiod and illumination at 10–25 °C. Misting was triggered every 20 min to ensure that plants remained well hydrated, growing on their original substrate during the course of the experimental work.

Hydraulic conductance. The efficiency of the water transport system was measured by subjecting plants to varying rates of evaporation and measuring the water potential gradient associated with transpiration (equation (1)):

$$K = F/\Delta\psi \quad (1)$$

where K = hydraulic conductance (mmol m^{-2} s^{-1} MPa^{-1}), F = hydraulic flux (measured as either evaporative loss from leaves or liquid intake into shoots (mmol m^{-2} s^{-1}) and $\Delta\psi$ = water potential difference between water source and leaves (MPa).

The hydraulic conductance of whole moss plants (K_{plant}), moss rhizomes/rhizoids (K_{root}) and moss shoot components was measured based on the theory that plant water transport functions as a series of connected resistors that can be excised and measured individually (equation (2)):

$$\frac{1}{K_{plant}} = \frac{1}{K_{root}} + \frac{1}{K_{shoot}} \quad (2)$$

Initially, K_{plant} was measured in six well-watered individuals by enclosing each individual entire moss canopy in an infrared gas analyser (Walz GFS3000) to attain steady-state transpiration under controlled conditions of 22 °C and 75% relative humidity, and illuminated at a saturating light intensity of 1,500 μmol photons m^{-2} s^{-1}. Plants were allowed to transpire until a steady rate of transpiration was recorded for 10 min. Once equilibrated, shoots were removed from the flowmeter, wrapped in moist paper towel and placed in a Scholander Pressure Chamber (PMS), where a balance pressure was used to determine shoot water potential (Ψ_{shoot}). Balance pressures were readily and repeatably determined and, in a subsample of five plants, a psychrometer (ICT) was used to verify Ψ_{shoot} determined by balance pressure in non-transpiring plants. Using equation (2), it was possible to calculate K_{plant} from the steady-state transpiration rate and with Ψ_{shoot} as the driving force (assuming that soil ψ was close to zero). Following the determination of K_{plant}, the excised shoots were trimmed and hydrated under water for 15 min before being attached to a hydraulic apparatus capable of measuring

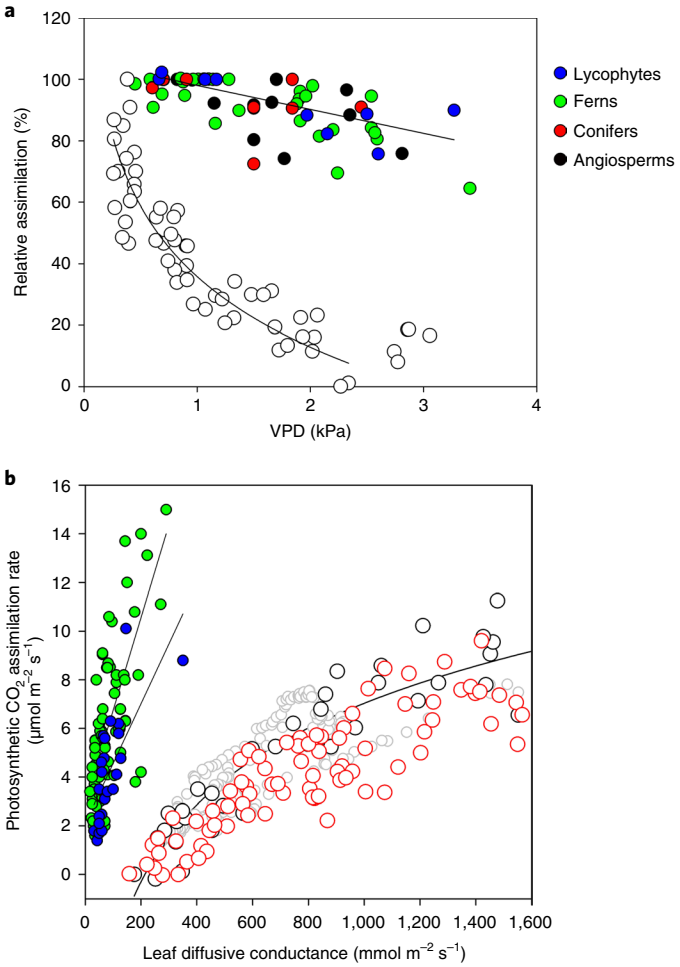

Fig. 4 | Compared to vascular plants, photosynthesis in *P. commune* is highly sensitive to humidity as a result of its intrinsically inefficient exchange of water vapour for CO_2. a, Sensitivity of photosynthesis in *P. commune* leaves to vapour pressure deficit (VPD) (open circles; curved line denotes least-squares log regression, $r^2 = 0.83$, $P < 0.001$) was very high, with assimilation approaching zero at a mild VPD of 2.5 kiloPascals (kPa). In contrast, a sample of vascular plants (Extended Data Fig. 9), including lycophytes (blue, $n = 3$), ferns (green, $n = 8$), conifers (red, $n = 4$) and angiosperms (black, $n = 7$), showed much lower sensitivity of relative assimilation (expressed as percentage of maximum assimilation recorded at VPD < 0.5 kPa) to VPD. A least-squares linear regression is fitted to vascular plant data ($r^2 = 0.61$, $P < 0.01$). **b**, A strong relationship between diffusive conductance to water vapour and photosynthetic rate in *P. commune* plants subjected to a range of humidity treatments (open circles, $n = 50$ individuals) or water stress (red circles, $n = 100$ individuals). Also shown are transient measurements made during dynamic transitions between different humidities (grey circles, least-squares log regression, $r^2 = 0.86$, $P < 0.0001$). In comparison, lycophytes (blue points, $n = 20$ species, Extended Data Fig. 9) and ferns (green points, $n = 64$ species, Extended Data Fig. 9) have a much higher intrinsic efficiency of water use (photosynthetic rate/leaf diffusive conductance) than moss, even across a similar range of photosynthetic rates.

very small liquid fluxes as water passed from a small reservoir into the base of the excised shoot[42]. Rates of water uptake were determined by a pressure transducer placed downstream of a large resistor (HPLC tubing) situated between a water reservoir and the shoot. A voltage logger (CR10X, Campbell Scientific) was used to monitor transducer output. Shoots were returned to the gas exchange cuvette under original conditions and allowed to transpire until water uptake was stable for 5–10 min. Shoots were then wrapped and returned to the pressure chamber to determine ψ and hence K_{shoot} using equation (2). Agreement between liquid and vapour fluxes was checked before calculations were made. Leaf areas were measured by removing leaves and using a flatbed scanner (Epson Perfection) and image analysis (ImageJ, NIH) to determine total projected leaf area per sample.

Conduit collapse. Scanning electron cryomicroscopy was used to observe the form of the water-conducting hydroids in *P. commune* in their native state when exposed to increasing tension in the water column as plants were dehydrated. Experiments were carried out at the Harvard University Imaging facility. Plants were slowly dehydrated on a bench and sampled periodically to provide a range of ψ. Before imaging, shoots were wrapped in moist paper towel and ψ measured using a Scholander pressure chamber (as above). Intact moss gametophytes were bench-dried for various lengths of time to generate a range of Ψ_{shoot}. The gametophytes were triple-bagged to prevent further water loss and allowed to equilibrate before ψ was measured. Samples were then frozen with a precooled (by liquid nitrogen) copper clamp and stored in liquid nitrogen. Short segments of the main axis were fixed in a custom sample holder while remaining submerged in liquid nitrogen. A cryotransfer Shuttle VCT 100 (Bal Tec) was used to transfer the sample to a precooled chamber under vacuum for fracturing and coating. The sample was fractured using a knife cooled to −150 °C, etched for 5–10 min depending on water content at −100 °C and sputter-coated with platinum at −130 °C with a BAL-TEC MED020 Coating System (Bal Tec). Samples were then imaged at an accelerating voltage of 3.0 kV in a Zeiss NVision 40 Dual-Beam focused ion beam and scanning electron microscope (SEM; Zeiss) with a cryogenic stage maintained at −150 °C.

Images of 14 individuals in various states of dehydration were analysed in ImageJ using a circularity metric ($C = 4\pi A/P^2$, where C = circularity, A = area and P = perimeter) to define the shape of conducting cells. Hydroids were identified by the fact that they contained water, which lacked the distinct surface features produced by adjacent living cells. Hydroids containing air were also counted, to determine whether cell shape was maintained when water tension was not locally present. All hydroids in the central region of the stem conducting strand were measured ($n > 50$ per stem), and hydroid shape was plotted relative to ψ exposure.

Hydroid vulnerability. Three techniques were used to determine the susceptibility of *P. commune*-conducting hydroids to cavitation. Each technique involved imaging the formation of gas embolisms in the lumen of hydroids as shoots became progressively dehydrated. The first technique used CryoSEM (described above). Images were analysed to determine the number of air-filled hydroids compared with the total number of hydroids in the conducting strand of the stem.

The second technique employed an optical technique to visualize cavitation in situ in real time. *P. commune* individuals were carefully removed from the soil to prevent any damage to the conductive tissue. Samples were then submerged under water in a Petri dish to allow full hydration and removal of attached substrate. At a distance of 5–10 cm from the base of the leaf, a region of the epidermal tissue of the stem was carefully removed under a dissecting microscope using a razor to expose the central conducting hydrome. Damage to hydroids was clearly visualized as an instantaneous colour change, and those samples were discarded. Samples were fixed on top of a piece of glass, covered with conductive adhesive gel and topped with a coverslip. The rhizoid of the moss sample was maintained in water while the sample was positioned under a microscope, and images were collected with an Axiocam (Carl Zeiss) digital camera connected to a microscope (Axioskop 2 Plus, Carl Zeiss) at ×100 magnification. Images from the stem hydrome were captured using transparent light every 30 s during the drying process under laboratory conditions (22 °C and ~60% relative humidity).

Once stable, the moss rhizome/rhizoids were removed from the water and the plant allowed to dehydrate. Hydroid cavitation was clearly observed during dehydration due to a very rapid change in local light transmittance in the region of the hydrome. Images were captured until at least 1 h from the last observed cavitation event. The cavitation profile of each sample of Image sequences was analysed following ref. [43]. Pixel differences between neighbouring images were first determined by subtracting the pixel values of each image from the next using ImageJ (see http://www.opensourceov.org/ for full details). This enabled cavitation events due to the reduction in transmission of light to the microscope camera. Noise not associated with cavitation events was then removed using the ImageJ outlier removal. The total embolism area per captured image was calculated as the sum of non-zero pixels and expressed as cumulative embolisms, a percentage of total embolism area in the sequence. Cavitation spread or propagation could be observed directly.

Given the difficulty of determining Ψ directly once the moss was set under the microscope, the relationship between Ψ and characteristic leaf movement towards the stem as plant water content decreased[44] was previously determined to be able to estimate the latter. To this end, *P. commune* individuals were horizontally displayed, photographed and Ψ was measured using a Scholander pressure chamber every 2–3 min from full hydration until its value became too negative to measure (<−10 MPa). Leaf angle was determined as the angle of the leaf blade to the vertical (represented by the stem) in 10–20 leaves at each step using ImageJ. An exponential growth regression was fitted with leaf angle and Ψ_{shoot}, allowing the

estimation of Ψ_{shoot} from leaf images (Extended Data Fig. 6). Thus, simultaneously with microscope image captures, orthogonal images of leaves of the horizontally displayed moss were collected with a digital camera every 3 min. Leaf angle was monitored at 10–20 leaves per individual using ImageJ, and the average value was used to estimate Ψ_{shoot} at each step. To derive moss Ψ at the time of microscope image capture, linear regressions were fitted between Ψ_{shoot} estimates and the time of digital camera image captures. Moss Ψ_{shoot} was plotted against cumulative embolisms (percentage of total), and P_{50} (Ψ at which 50% of the hydrome cavitation events had been observed) was determined by fitting a sigmoid using equation (3) (ref. [45]):

$$\text{Cumulative embolisms} = 100\ (1 + e^{(a(\Psi - P_{50}))}) \quad (3)$$

P_{50} was derived for each of the ten replicates. Spatio-temporal colour maps of cavitation formation were created for a single replicate by colouring the embolism area in each sequence using a colour scale of Ψ_{shoot} over time (Fig. 2).

The third visualization technique used to image moss hydroids was X-ray micro-computed tomography. Using this technique, direct visualization of embolized hydroids in the stems of intact mosses was carried out during tomography campaigns in 2017 at the PSICHE beamline of the SOLEIL synchrotron, France[46]. Tomographic observations were conducted using a high-flux (3×10^{11} photons mm^{-2}) 25-keV monochromatic X-ray beam with rotation from 0° to 180° using a continuous rotation mode. X-ray projections were collected with a 50-ms exposure time during rotation and recorded with an Orca-flash sCMOS camera (Hamamatsu Photonics) equipped with a 250-µm-thick LuAG scintillator. Whole moss plants ($n = 12$) were dried for different lengths of time (2–30 min) on a laboratory bench and carefully wrapped in wet paper and plastic foil to prevent further dehydration during scans, then fixed to the rod with tape to allow free rotation of the sample over 180°. The scan time was 75 s for each sample, and this yielded a stack of 1,500 TIFF image slices. Tomographic reconstructions were conducted using the Paganin method[47] in PyHST2 software[48] and resulted in two-bit volumic images with 0.9-µm^3 voxel resolution. We measured Ψ_{shoot} immediately after the scan with a Scholander pressure bomb (SAM Precis) using the scanned stem still wrapped in wet paper and plastic foil. Each moss stem was scanned once only. Analysis of images was undertaken using a composite of five images from the centre of each image stack. Cavitated conduits were readily identified and counted. Water-filled hydroids in the central hydrome were identified by their large lumina, thick walls and paired arrangement. A mean number of functional hydroids per stem ($n = 15$) was determined in fully cavitated samples, and the number of cavitated hydroids in each sample expressed as a percentage of this mean.

Refilling. A single individual was wetted following cavitation, to examine refilling in the same hydroids used to observe cavitation during drying. This involved adding water to the rhizome and leaves of the plant while recording images as above. The collapse of bubbles through time could readily be visualized and quantified using ImageJ to measure the remaining volume of air in individual hydroids as they filled.

In addition to direct visualization of cavitation in hydroids, a hydraulic technique was used to examine the effects of dehydration on water transport efficiency (hydraulic conductance) of the moss shoot. A sample of 20 individuals was carefully removed intact from the soil and allowed to dehydrate for 0–30 min to create a range of ψ between −0.05 and 3.4 MPa. These shoots were excised under water, connected to the hydraulic apparatus described above and allowed to transpire for 6 min under saturating light (1,500 µmol photons m^{-2} s^{-1}) at 22 °C and 50% relative humidity. Shoots were quickly removed from the flowmeter, and Ψ_{shoot} and leaf area measured as above to allow calculation of shoot hydraulic conductance using equation (1).

Gas exchange response to dehydration. Changes in the diffusive conductance of *P. commune* shoots to water vapour in plants subjected to various degrees of dehydration were measured using an open-flow gas exchange system (Walz GFS). All leaves in a shoot were enclosed in the cuvette, ensuring that there was no path for external flow between soil and leaves (see boxed region in Fig. 2a) and that leaves maintained good contact with the cuvette thermocouple. Shoots remained attached to the soil and were allowed to reach equilibrium transpiration rates under conditions of high light (1,500 µmol m^{-2} s^{-1}) and optimum cuvette temperature (22 °C). Before measurement, all plants were equilibrated overnight at very high humidity by bagging blocks of individuals, thus establishing leaves in a humidified state but without liquid water on the plant surface. Humidity in the cuvette was maintained at approximately 80%, and gas exchange parameters recorded once evaporative and photosynthetic fluxes became stable (<2% variation over 5 min). At this point, shoots were excised and quickly wrapped in moist paper towel and Ψ_{shoot} measured with a Scholander pressure chamber. To extend the range of Ψ_{shoot} exposure, some shoots were either allowed to dry over several days in soil or excised from the soil and allowed to desiccate in the cuvette for up to 15 min at a humidity of 75% before gas exchange and Ψ_{shoot} were measured. Following measurements, all shoots were placed in water to rehydrate and leaf area measured on a scanner as above, allowing normalization of gas exchange measurements to the projected leaf area. Measurements were carried out on 100 specimens sampled from the larger (more emergent) plants within a large colony.

Gas exchange response to evaporative demand. Changes in diffusive conductance and photosynthetic CO_2 uptake of *P. commune* shoots in response to changes in humidity were measured using two gas exchange systems with high-precision cuvette humidity control (Walz GFS and Licor 6800). Entire blocks of plants were equilibrated overnight under conditions maintained slightly below condensing humidity, but with leaves completely dry and soil well hydrated. All leaves were enclosed in the cuvette under the same light and temperature conditions as above, but with cuvette humidity regulated to a range of values by modifying influx vapour pressure. Shoots were initially equilibrated to a high humidity (>80%), ensuring that the cuvette temperature was slightly warmer than ambient air conditions and that the heat exchanger on the cuvette was maintained outside the condensing range of temperature. Initial high-humidity conditions were closely monitored for 10 min to ensure that no cuvette water adsorption or plant surface water was evident (identified by non-stable readings or an atypical ratio of A/g). Following high-humidity treatment, cuvette humidity was lowered to a value between 70 and 10% and a single value of gas exchange recorded after an equilibration period of >15 min. A group of five plants were additionally monitored during a series of humidity transitions to understand the dynamics of the gas exchange response, and to determine the dynamic recovery of gas exchange upon returning to high humidity. Dynamic ($n = 5$ plants) and steady-state ($n = 50$ plants) gas-exchange parameters were recorded, as well as Photosystem II quantum yield, determined by exposing shoots to a saturating flash while recording chlorophyll fluorescence emission.

Hydraulic model. The capacity of *P. commune* to function under varying humidity conditions was modelled to determine how closely moss plants operated to hydraulic failure, and the importance of regulation of transpiration for the maintenance of photosynthesis as humidity falls.

The hydraulic model electrical circuit analogy[49] for plant-based water relations was used to calculate the water potential gradient within the plant ($\Delta\psi$), based on Ohm's law from the transpiration rate and the hydraulic conductance of the whole plant (K_{moss}):

$$\Delta\Psi = Dg_{moss}/K_{moss} \quad (4)$$

where D = vapour pressure deficit and g_{moss} = moss diffusive conductance to water vapour. Given that plants were growing on a fully hydrated substrate, it was possible to determine maximum possible g_{moss}:

$$g_{moss} = \Psi K_{moss}/D \quad (5)$$

where Ψ = leaf water potential. However, due to the vulnerability of the moss water transport system to cavitation, K_{moss} is sensitive to ψ according to an empirically determined sigmoidal function (Extended Data Fig. 3):

$$\left(K_{moss} = A/\left(1 + e^{(-(\psi - \psi o)/b))}\right)\right. \quad (6)$$

Additionally, it was possible to predict the assimilation of the moss using a well-defined empirical relationship between A and g_{moss} determined from measurements of *P. commune* under a range of humidities and hydration states with saturating light (Fig. 4).

Two simulations were run to describe (1) the impact of relative humidity on A assuming no regulation of g_{moss} (as expected according to the lack of stomatal regulation valves); and (2) the impact of relative humidity assuming that g_{moss} was regulated to maintain ψ in the non-cavitating range (−1.1 MPa). A range of humidity from 5 to 90% was simulated, with air temperature fixed at 22 °C and a simplifying assumption that leaf and air temperature were equal.

Reporting Summary. Further information on research design is available in the Nature Research Reporting Summary linked to this article.

Data availability

All processed data are contained in the manuscript or Extended Data. Raw images and image sequences can be supplied upon request from the corresponding author.

Received: 14 August 2019; Accepted: 22 January 2020;
Published online: 9 March 2020

References

1. Kenrick, P. & Crane, P. R. The origin and early evolution of plants on land. *Nature* **389**, 33–39 (1997).
2. Edwards, D., Davies, K. L. & Axe, L. A vascular conducting strand in the early land plant *Cooksonia*. *Nature* **357**, 683–685 (1992).
3. Lang, W. H. IV—On the plant-remains from the Downtonian of England and Wales. *Philos. Trans. R. Soc. Lond. B* **227**, 245–291 (1937).
4. Renzaglia, K., McFarland, K. & Smith, D. Anatomy and ultrastructure of the sporophyte of *Takakia ceratophylla* (Bryophyta). *Am. J. Bot.* **84**, 1337–1350 (1997).

5. Stein, W. E., Mannolini, F., Hernick, L. V., Landing, E. & Berry, C. M. Giant cladoxylopsid trees resolve the enigma of the Earth's earliest forest stumps at Gilboa. *Nature* **446**, 904–907 (2007).
6. Harrison, C. J. & Morris, J. L. The origin and early evolution of vascular plant shoots and leaves. *Phil. Trans. R. Soc. Lond. B* **373**, 20160496 (2017).
7. Carlquist, S. J. *Ecological Strategies of Xylem Evolution* (Univ. of California Press, 1975).
8. Raven, J. A. Evolution of vascular land plants in relation to supracellular transport processes. *Adv. Bot. Res.* **5**, 153–219 (1977).
9. Duckett, J. G. & Pressel, S. The evolution of the stomatal apparatus: intercellular spaces and sporophyte water relations in bryophytes—two ignored dimensions. *Phil. Trans. R. Soc. B* **373**, 20160498 (2017).
10. Bowman, J. L. et al. Insights into land plant evolution garnered from the *Marchantia polymorpha* genome. *Cell* **171**, 287–304 (2017).
11. Xu, B. et al. Contribution of NAC transcription factors to plant adaptation to land. *Science* **343**, 1505–1508 (2014).
12. Honkanen, S., Thamm, A., Arteaga-Vazquez, M. A. & Dolan, L. Negative regulation of conserved RSL class I bHLH transcription factors evolved independently among land plants. *eLife* **7**, e38529 (2018).
13. Ohtani, M., Akiyoshi, N., Takenaka, Y., Sano, R. & Demura, T. Evolution of plant conducting cells: perspectives from key regulators of vascular cell differentiation. *J. Exp. Bot.* **68**, 17–26 (2017).
14. Hébant, C. *The Conducting Tissues of Bryophytes* (J. Cramer, 1977).
15. Edwards, D., Axe, L. & Duckett, J. Diversity in conducting cells in early land plants and comparisons with extant bryophytes. *Bot. J. Linn. Soc.* **141**, 297–347 (2003).
16. Haberlandt, G. Beiträge zur Anatomie und Physiologie der Laubmoose. *Jahrb. Wiss. Bot.* **17**, 359–498 (1886).
17. Tansley, A. G. & Chick, E. Notes on the conducting tissue-system in Bryophyta. *Ann. Bot.* **15**, 1–38 (1901).
18. Atala, C. Water transport and gas exchange in the non-vascular plant *Dendroligotrichum dendroides* (Brid. ex Hedw.) Broth. (Polytrichaceae, Bryophyta). *Gayana Bot.* **68**, 89–92 (2011).
19. Blaikley, N. M. Absorption and conduction of water and transpiration in *Polytrichum commune*. *Ann. Bot.* **46**, 289–300 (1932).
20. Ligrone, R., Duckett, J. & Renzaglia, K. Conducting tissues and phyletic relationships of bryophytes. *Phil. Trans. R. Soc. Lond. B* **355**, 795–813 (2000).
21. Vanderpoorten, A. & Goffinet, B. *Introduction to Bryophytes* (Cambridge Univ. Press, 2009).
22. Tyree, M. T. & Zimmermann, M. H. *Xylem Structure and the Ascent of Sap* (Springer Science & Business Media, 2013).
23. Weng, J. K. & Chapple, C. The origin and evolution of lignin biosynthesis. *New Phytol.* **187**, 273–285 (2010).
24. Espiñeira, J. et al. Distribution of lignin monomers and the evolution of lignification among lower plants. *Plant Biol.* **13**, 59–68 (2011).
25. Martin StPaul, N., Delzon, S. & Cochard, H. Plant resistance to drought depends on timely stomatal closure. *Ecol. Lett.* **20**, 1437–1447 (2017).
26. Ligrone, R., Carafa, A., Duckett, J., Renzaglia, K. & Ruel, K. Immunocytochemical detection of lignin-related epitopes in cell walls in bryophytes and the charalean alga *Nitella*. *Plant Syst. Evol.* **270**, 257–272 (2008).
27. Brodribb, T. J., Feild, T. S. & Jordan, G. J. Leaf maximum photosynthetic rate and venation are linked by hydraulics. *Plant Physiol.* **144**, 1890–1898 (2007).
28. Becker, P., Tyree, M. T. & Tsuda, M. Hydraulic conductances of angiosperms versus conifers: similar transport sufficiency at the whole-plant level. *Tree Physiol.* **19**, 445–452 (1999).
29. Sperry, J. S. & Tyree, M. T. Mechanism of water stress-induced xylem embolism. *Plant Physiol.* **88**, 581–587 (1988).
30. Choat, B. et al. Global convergence in the vulnerability of forests to drought. *Nature* **491**, 752 (2012).
31. Lenne, T., Bryant, G., Hocart, C. H., Huang, C. X. & Ball, M. C. Freeze avoidance: a dehydrating moss gathers no ice. *Plant Cell Environ.* **33**, 1731–1741 (2010).
32. Cardoso, A. A., Brodribb, T. J., Lucani, C. J., DaMatta, F. M. & McAdam, S. A. Coordinated plasticity maintains hydraulic safety in sunflower leaves. *Plant Cell Environ.* **41**, 2567–2576 (2018).
33. Cochard, H., Casella, E. & Mencuccini, M. Xylem vulnerability to cavitation varies among poplar and willow clones and correlates with yield. *Tree Physiol.* **27**, 1761–1767 (2007).
34. Rolland, V. et al. Easy come, easy go: capillary forces enable rapid refilling of embolized primary xylem vessels. *Plant Physiol.* **168**, 1636–1647 (2015).
35. Cochard, H., Coll, L., Le Roux, X. & Améglio, T. Unraveling the effects of plant hydraulics on stomatal closure during water stress in walnut. *Plant Physiol.* **128**, 282–290 (2002).
36. Brodribb, T. J. & McAdam, S. A. Evolution of the stomatal regulation of plant water content. *Plant Physiol.* **174**, 639–649 (2017).
37. Bayfield, N. G. Notes on water relations of *Polytrichum commune* Hedw. *J. Bryol.* **7**, 607–617 (1973).
38. Clayton-Greene, K., Collins, N., Green, T. & Proctor, M. Surface wax, structure and function in leaves of Polytrichaceae. *J. Bryol.* **13**, 549–562 (1985).
39. Carriquí, M. et al. Anatomical constraints to non-stomatal diffusion conductance and photosynthesis in lycophytes and bryophytes. *New Phytol.* https://doi.org/10.1111/nph.15675 (2019).
40. Pressel, S. & Duckett, J. G. Do motile spermatozoids limit the effectiveness of sexual reproduction in bryophytes? Not in the liverwort *Marchantia polymorpha*. *J. Syst. Evol.* **57**, 371–381 (2019).
41. Essig, F. B. *Plant Life: A Brief History* (Oxford Univ. Press, 2015).
42. Brodribb, T. J. & Cochard, H. Hydraulic failure defines the recovery and point of death in water-stressed conifers. *Plant Physiol.* **149**, 575–584 (2009).
43. Brodribb, T. J., Carriqui, M., Delzon, S. & Lucani, C. Optical measurement of stem xylem vulnerability. *Plant Physiol.* **174**, 2054–2061 (2017).
44. Sarafis, V. A biological account of *Polytrichum commune*. *N. Z. J. Bot.* **9**, 711–724 (1971).
45. Pammenter, Nv & Van der Willigen, C. A mathematical and statistical analysis of the curves illustrating vulnerability of xylem to cavitation. *Tree Physiol.* **18**, 589–593 (1998).
46. King, A. et al. Tomography and imaging at the PSICHE beam line of the SOLEIL synchrotron. *Rev. Sci. Instrum.* **87**, 093704 (2016).
47. Paganin, D., Mayo, S., Gureyev, T. E., Miller, P. R. & Wilkins, S. W. Simultaneous phase and amplitude extraction from a single defocused image of a homogeneous object. *J. Microsc.* **206**, 33–40 (2002).
48. Mirone, A., Brun, E., Gouillart, E., Tafforeau, P. & Kieffer, J. The PyHST2 hybrid distributed code for high speed tomographic reconstruction with iterative reconstruction and a priori knowledge capabilities. *Nucl. Instrum. Methods Phys. Res. B* **324**, 41–48 (2014).
49. Van den Honert, T. Water transport in plants as a catenary process. *Discuss. Faraday Soc.* **3**, 146–153 (1948).

Acknowledgements

We thank A. Graham at the Harvard Center for Nanoscale Studies for his expert technical assistance with Cryo-SEM. We acknowledge the SOLEIL synchrotron, Saclay, France for provision of synchrotron radiation beamtime at the PSICHE beamline, and thank A. King for assistance. This research was funded by an Australian Research Council Discovery Grant (no. DP 170100761 awarded to T.J.B.). M.C. received a travel grant from La Caixa Banking Foundation and from the Conselleria d'Educació i Universitats (Govern de les Illes Balears) and European Social Fund (predoctoral fellowship no. FPI/1700/2014). N.M.H. was supported by a Visiting Scholar award from the University of Tasmania, and NSF grants nos. IOS-1659918 and DMR-1420570 studies. This work was supported by the programme Investments for the Future (nos. ANR-10-EQPX-16, XYLOFOREST and Labex COTE) from the French National Agency for Research.

Author contributions

T.J.B., M.C. and N.M.H. designed the study. T.J.B., N.M.H., M.C. and S.D. carried out the experiments. T.J.B. wrote the manuscript with input from N.M.H., M.C., S.D. and S.A.M.M. S.A.M.M. provided additional data.

Competing interests

The authors declare they have no competing interests.

Additional information

Extended data is available for this paper at https://doi.org/10.1038/s41477-020-0602-x.

Supplementary information is available for this paper at https://doi.org/10.1038/s41477-020-0602-x.

Correspondence and requests for materials should be addressed to T.J.B. or N.M.H.

Peer review information Nature Plants thanks Jeffrey Duckett, Karen Renzaglia and the other, anonymous, reviewer for their contribution to the peer review of this work.

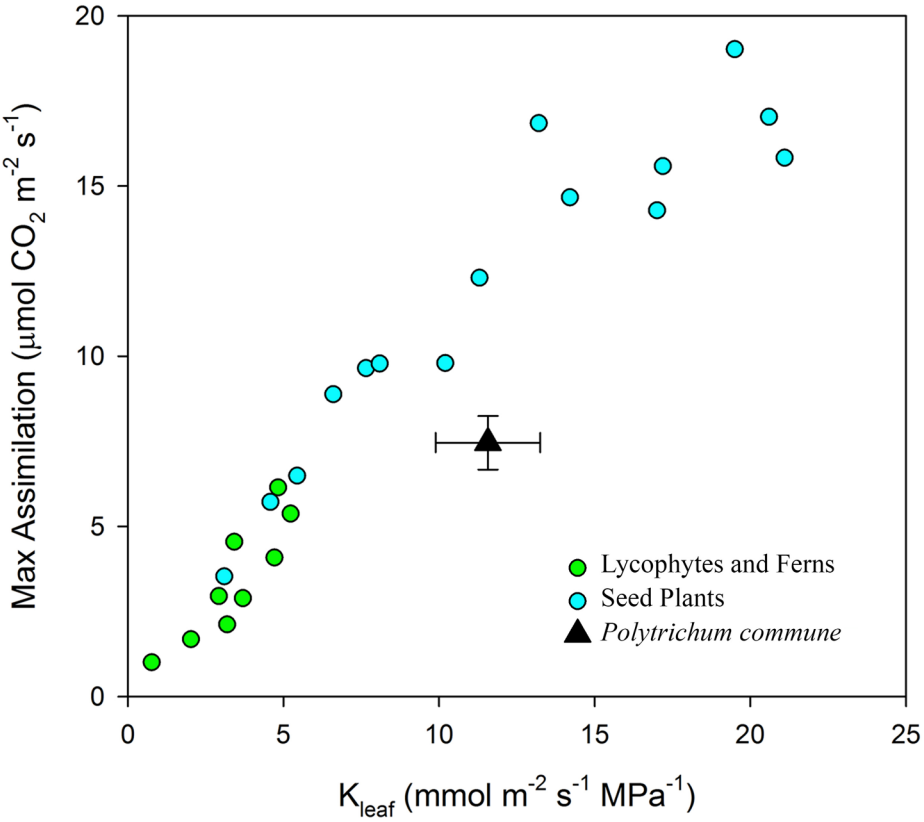

Extended Data Fig 1 | Coordinated hydraulic conductance and assimilation. The mean shoot hydraulic conductance and mean photosynthetic capacity of *Polytrichum commune* (+/- SD, n = 7 individuals) measured here (triangle) falls close to the relationship found in leaves from the major groups of vascular plants; lycophytes and ferns (green), seed plants (blue) (published data from (27)).

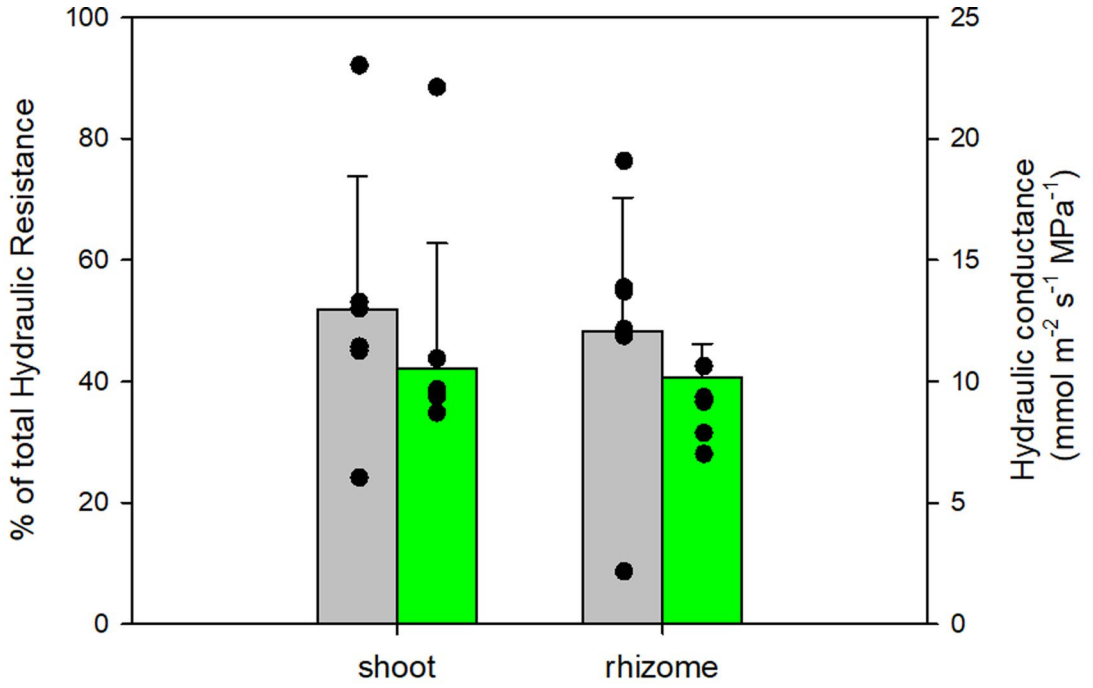

Extended Data Fig 2 | Above and below ground hydraulic resistance. The distribution of hydraulic resistances as a percentage of total resistance (grey bars + SD, n = 7) between belowground (rhizoid) and aboveground (shoot) tissues in *Polytrichum commune* plants. Absolute values of hydraulic conductance (means shown as green bars, + SD, n = 7) show considerable variation, but the split between tissues is similar.

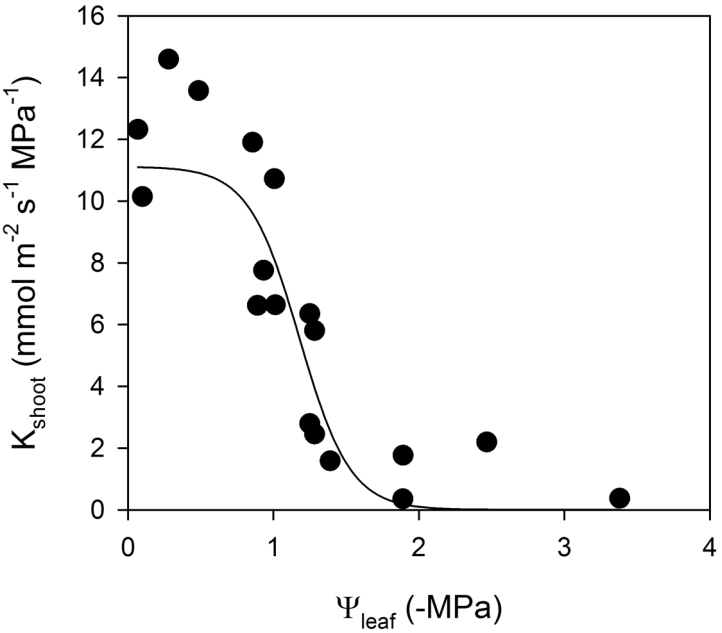

Extended Data Fig 3 | Shoot hydraulic vulnerability. The hydraulic conductance of *Polytrichum commune* shoots (K_{shoot}) was observed to decline sharply upon exposure to water stress. Each point represents a separate plant (n = 18 individuals) subjected to different degrees of dehydration stress. A rapid decline of K_{shoot} between -1 and −2MPa matched the observed pattern of cavitation using visual methods (Fig. 2). The form of the sigmoidal function fitted here was used in the hydraulic model used in Fig. 3.

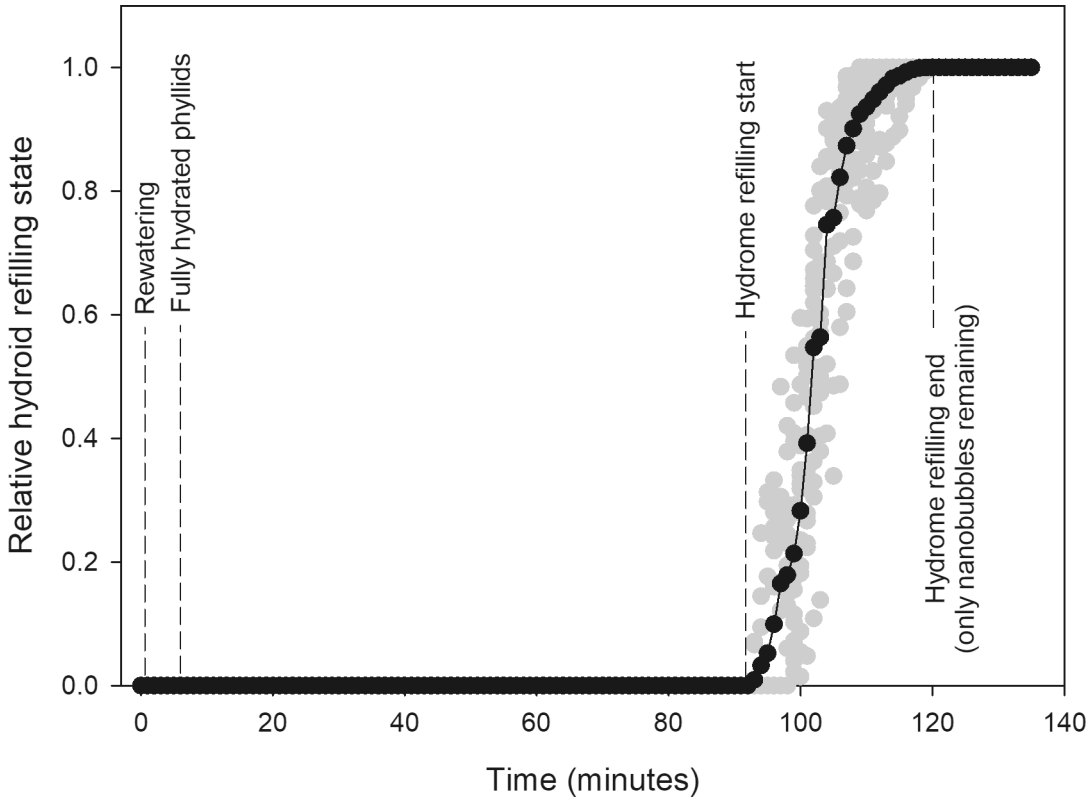

Extended Data Fig 4 | Refilling kinetics in *Polytrichum*. Hydroids of the central strand of a single *Polytrichum commune* caulidium are shown to refill after a droughted plant that had fully cavitated was rehydrated after several hours (>12) after the last cavitation event was observed. Data from a single individual stem from an intact plant shows that 90 min after rewatering from both phyllidia and rhizome the hydroids begin to effectively refill with water, compressing the air into nanobubbles (which should dissolve over time) at around 125 min after rewatering of the plant. Average relative hydroid refilling state (proportion of water present in hydroids) over time is shown as black dots, while individual hydroid refilling states for each hydroid are shown as grey dots.

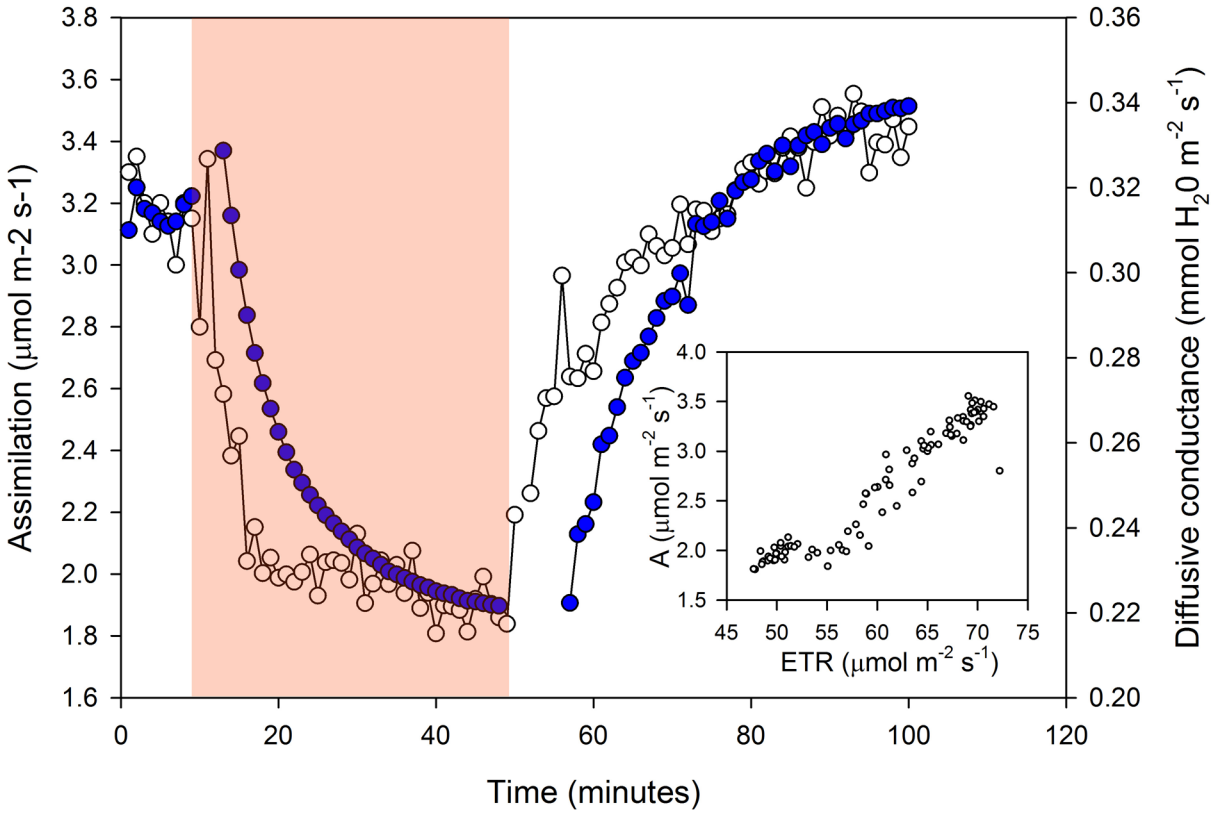

Extended Data Fig 5 | Dynamic response to humidity in *Polytrichum* gas exchange. Dynamic changes in photosynthetic assimilation rate and leaf diffusive conductance to water vapor during a transition from a vapor pressure deficit of 1.5 kPa (approximately 50% RH) to 3 kPa (approximately 5% RH). The pink box shows measurements made at 3 kPa, after which vapor pressure deficit was decreased to 1.0 kPa and recovery recorded. A rapid reduction in diffusive conductance and photosynthesis is evident upon exposure to drier air, while a complete recovery occurs upon return to more humid conditions. Changes in photosynthetic assimilation (A) measured by gas analysis correspond with changes in photosynthetic electron transport rate (ETR) measured by chlorophyll fluorescence (graph insert).

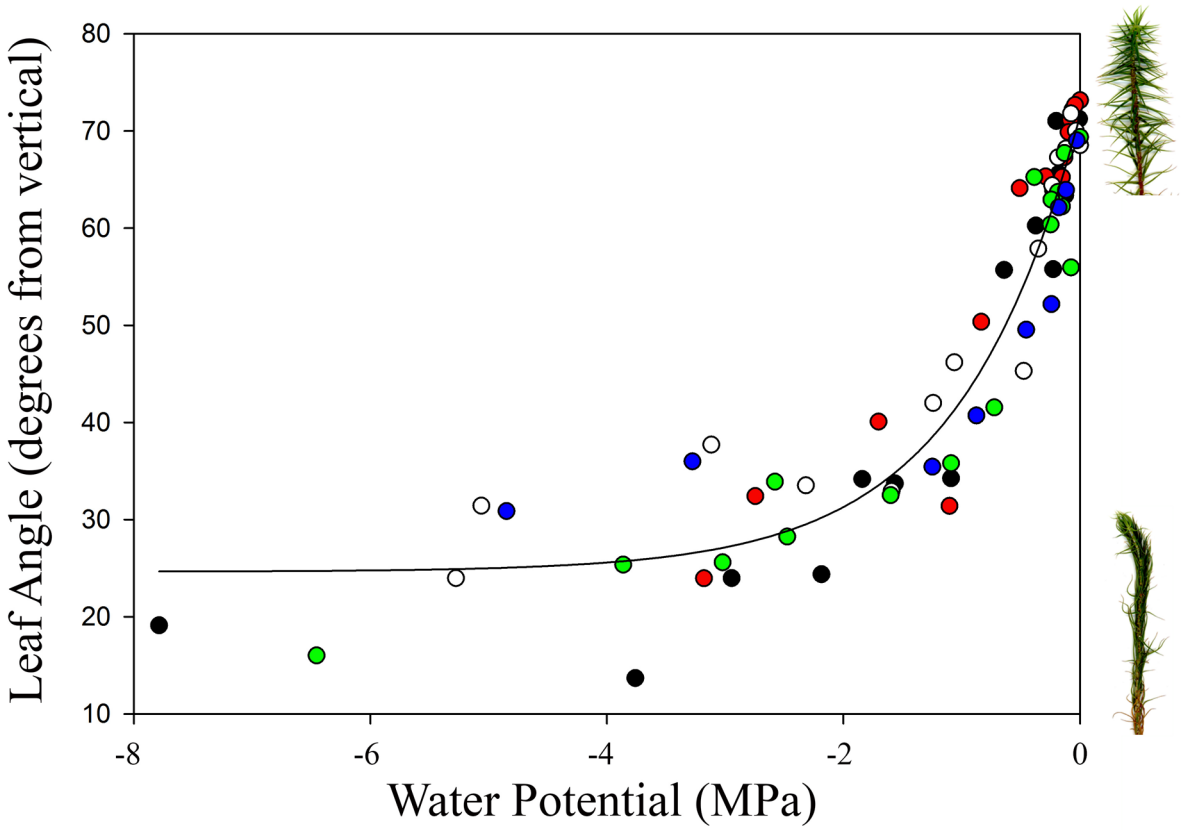

Extended Data Fig 6 | Leaf movement in response to dehydration in *Polytrichum*. As shoots of *Polytrichum commune* desiccate, leaves move from a position that is perpendicular to the stem (image top right) to being arranged parallel to the stem (image lower right). The relationship between leaf angle and ψ_{shoot} for five individuals subjected to slow desiccation (each color represents a different replicate plant) shows a rapid decline in leaf angle as ψ_{shoot} fell from 0 to −1.5 MPa. This pattern of decline matched closely the pattern of declining diffusive conductance seen in Fig. 3.

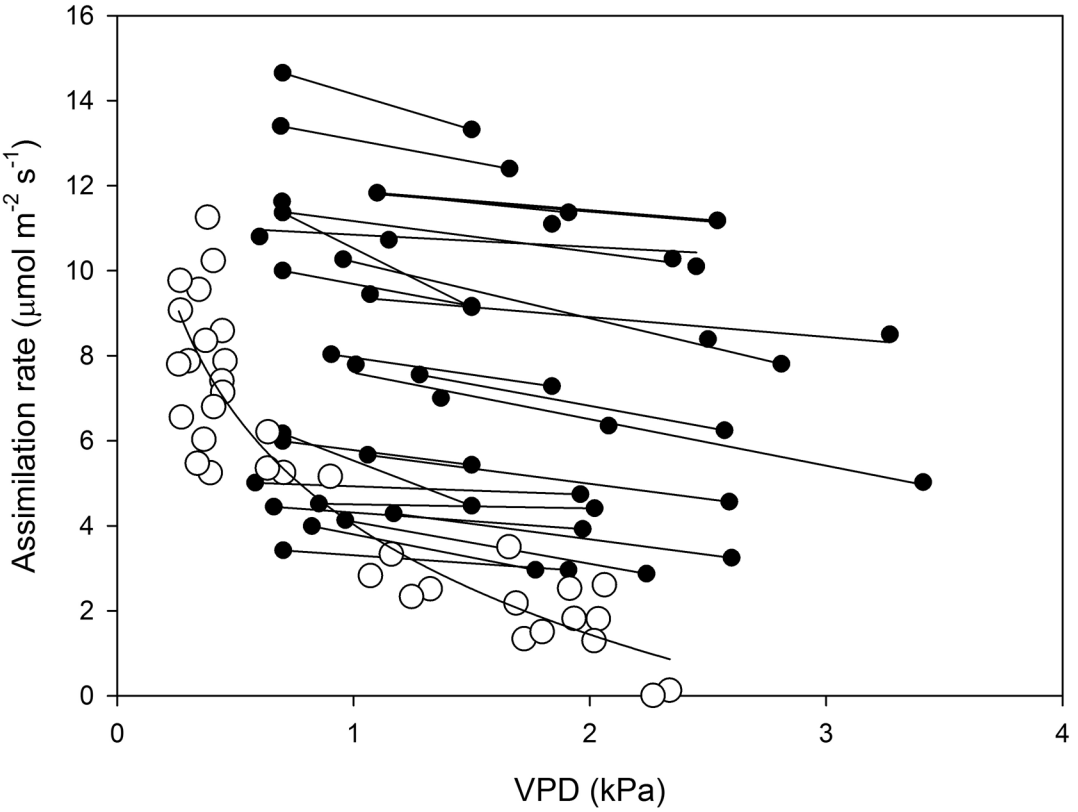

Extended Data Fig 7 | Humidity sensitivity of assimilation. Sensitivity of absolute assimilation rate to *VPD* in *P. commune* (open circles) and vascular plants (black points).

Family	Species	Vapour pressure difference (kPa)	Photosynthetic rate (μmol m^{-2} s^{-1})	Stomatal conductance (mol m^{-2} s^{-1})	Source
		LYCOPHYTES			
Selaginellaceae	*Selaginella kraussiana*	1.17	4.08	0.275	50
		2.15	3.19	0.186	
		2.6	3.03	0.144	
Selaginellaceae	*Selaginella uncinata*	0.663	4.45	0.119	51
		0.687	4.56	0.121	
		1.97	4.45	0.072	
Lycopodiaceae	*Lycopodium deuterodensum*	1.07	8.75	0.112	52
		2.5	7.74	0.096	
		3.27	7.79	0.088	
		FERNS			
Blechnaceae	*Blechnum nudum*	0.584	5.01	0.136	51
		0.69	4.77	0.13	
		1.96	4.74	0.0978	
Davalliaceae	*Davallia solida*	0.611	3.42	0.0462	51
		0.703	3.11	0.045	
		1.91	2.96	0.031	
Dennstaedtiaceae	*Pteridium esculentum*	1.1	12.19	0.167	52
		1.91	11.33	0.119	
		2.54	9.95	0.105	
Dicksoniaceae	*Dicksonia antarctica*	1.01	8.28	0.144	52
		1.37	6.38	0.118	
		2.08	5.65	0.078	
		3.41	4.85	0.059	
Dryopteridaceae	*Rumohra adiantiformis*	0.876	4.88	0.094	50
		1.06	4.99	0.072	
		2.59	4.19	0.051	
Polypodiaceae	*Pyrrosia lingua*	0.965	3.98	0.0278	50
		1.16	4.12	0.0255	
		2.24	3.64	0.0155	
Pteridaceae	*Adiantum capillus-veneris*	0.89	7.82	0.157	50
		1.28	8.28	0.147	
		2.57	6.67	0.075	
Pteridaceae	*Cheilanthes myriophylla*	0.854	5.17	0.117	50
		1.14	5.1	0.109	
		1.88	4.65	0.077	
		GYMNOSPERMS			
Cupressaceae	*Callitris rhomboidea*	0.603	10.8	0.22	51
		1.84	11.1	0.187	
		2.45	10.1	0.139	
Cupressaceae	*Metasequoia glyptostroboides*	0.906	8.03	0.151	53
		1.84	7.28	0.0848	
		2.11	7.1	0.077	
Pinaceae	*Pinus caribaea*	0.7	14.65	0.465	54
		1.5	13.32	0.18	
Podocarpaceae	*Prumnopitys ladei*	0.7	6.17	0.107	54
		1.5	4.47	0.0438	
		ANGIOSPERMS			
Amborellaceae	*Amborella trichopoda*	0.7	5.99	0.178	54
		1.5	5.43	0.0521	
Asteraceae	*Dahlia hybrida*	0.7	11.36	0.454	54
		1.5	9.13	0.205	
Brassicaceae	*Arabidopsis thaliana*	0.801	3.99	0.255	51
		1.77	3.33	0.682	
Fabaceae	*Pisum sativum*	0.69	13.4	0.496	51
		1.66	12.4	0.251	
Fagaceae	*Quercus robur*	0.7	10	0.246	54
		1.5	9.17	0.135	
Nothofagaceae	*Nothofagus cunninghamii*	0.698	11.62	0.203	51
		1.15	10.72	0.142	
		2.35	10.27	0.112	
Oleaceae	*Olea europaea*	0.956	10.26	0.324	51
		1.7	10.29	0.337	
		2.81	7.8	0.129	

Extended Data Fig. 8 | See next page for caption.

Extended Data Fig 8 | Table of humidity sensitivity in diverse species. Steady state leaf gas exchange across variable vapor pressure differences for vascular plant species taken from the literature.

50. McAdam, S. A. M. & Brodribb, T. J. Ancestral stomatal control results in a canalization of fern and lycophyte adaptation to drought. *New Phytol.* **198**, 429–441 (2013).
51. McAdam, S. A. M. & Brodribb, T. J. Linking turgor with ABA biosynthesis: implications for stomatal responses to vapour pressure deficit across land plants. *Plant Physiol.* **171**, 2008–2016 (2016).
52. Brodribb, T. J. & McAdam, S. A. M. Passive origins of stomatal control in vascular plants. *Science* **331**, 582–585 (2011).
53. McAdam, S. A. M. & Brodribb, T. J. Separating active and passive influences on stomatal control of transpiration. *Plant Physiol.* **164**, 1578–1586 (2014).
54. McAdam, S. A. M. & Brodribb, T. J. The evolution of mechanisms driving the stomatal response to vapour pressure deficit. *Plant Physiol.* **167**, 833–843 (2015).

Family	Species	Photosynthetic rate (μmol m^{-2} s^{-1})	Stomatal conductance (mol m^{-2} s^{-1})	Source
	LYCOPHYTES			
Selaginellaceae	*Selaginella anceps*	3.1	0.07	55
Selaginellaceae	*Selaginella arthritica*	3.4	0.08	55
Selaginellaceae	*Selaginella atirrensis*	1.8	0.06	55
Selaginellaceae	*Selaginella bryopteris*	8.8	0.35	56
Selaginellaceae	*Selaginella eurynota*	5.8	0.12	55
Selaginellaceae	*Selaginella goudotiana*	4.8	0.127	unpub
Selaginellaceae	*Selaginella kraussiana*	1.8	0.031	unpub
Selaginellaceae	*Selaginella martensii*	2.5	0.059	unpub
Selaginellaceae	*Selaginella moellendorffii*	4.2	0.06	57
Selaginellaceae	*Selaginella oaxacana*	2.4	0.05	55
Selaginellaceae	*Selaginella pallescens*	10.1	0.145	27
`Selaginellaceae	*Selaginella sp.*	2.1	0.05	55
Selaginellaceae	*Selaginella umbrosa*	3.5	0.1	55
Lycopodiaceae	*Dendrolycopodium dendroideum*	5.7	0.065	58
Lycopodiaceae	*Diphasiastrum digitatum*	5.6	0.07	unpub
Lycopodiaceae	*Hupersia varia*	3.5	0.05	unpub
Lycopodiaceae	*Lycopodium annotinum*	6.3	0.091	58
Lycopodiaceae	*Lycopodium clavatum*	6.2	0.12	58
Lycopodiaceae	*Lycopodium deuterodensum*	4.8	0.067	unpub
	FERNS			
Aspleniaceae	*Asplenium scolopendrium*	3.5	0.032	59
Aspleniaceae	*Asplenium trichomanes*	5.9	0.053	59
Aspleniaceae	*Asplenium trichomanes*	5.2	0.035	59
Athyriaceae	*Diplazium striatastrum*	4.2	0.2	55
Blechnaceae	*Blechnum gibbum*	4.9	0.036	59
Blechnaceae	*Blechnum magellanicum*	3.1	0.026	59
Blechnaceae	*Blechnum mochaenum*	3.3	0.05	59
Blechnaceae	*Blechnum penna-marina*	5.3	0.07	59
Cyatheaceae	*Cyathea mertensiana*	6	0.12	57
Cystopteridaceae	*Cystopteris sudetica*	6	0.124	59
Cystopteridaceae	*Gymnocarpium dryopteris*	5.7	0.058	59
Dennstaedtiaceae	*Hypolepis poeppigii*	4.4	0.025	59
Dennstaedtiaceae	*Pteridium aquilinum*	7.9	0.112	59
Dennstaedtiaceae	*Pteridium aquilinum*	10.6	0.085	59
Dennstaedtiaceae	*Pteridium aquilinum*	10.8	0.177	59
Dicksoniaceae	*Lophosoria quadripinnata*	5.5	0.036	59
Dryopteridaceae	*Bolbitis portoricensis*	3.2	0.06	55
Dryopteridaceae	*Dryopteris carthusiana*	5.6	0.064	59
Dryopteridaceae	*Dryopteris erythrosora*	4.7	0.05	59
Dryopteridaceae	*Dryopteris filix-mas*	3.4	0.017	59
Dryopteridaceae	*Dryopteris filix-mas*	6.4	0.062	59
Dryopteridaceae	*Dryopteris tyrrhena*	6.8	0.063	59
Dryopteridaceae	*Polystichum aculeatum*	6.2	0.048	59
Equisetaceae	*Equisetum arvense*	12	0.15	59
Equisetaceae	*Equisetum hyemale*	8.5	0.08	57
Equisetaceae	*Equisetum pratense*	8	0.142	59
Equisetaceae	*Equisetum sylvaticum*	6.8	0.126	59
Equisetaceae	*Equisetum telmateia*	13.7	0.143	59
Gleicheniaceae	*Dicranopteris linearis*	2	0.03	57
Gleicheniaceae	*Gleichenia squamulosa*	3.7	0.033	59
Lomariopsidaceae	*Cyclopeltis semicordata*	2.2	0.07	55
Lomariopsidaceae	*Lomariopsis japurensis*	3.3	0.07	55
Lygodiaceae	*Lygodium japonicum*	4.3	0.067	59
Marattiaceae	*Angiopteris lygodiifolia*	2.2	0.028	57
Nephrolepidaceae	*Nephrolepsis exaltata*	2.9	0.025	59
Onocleaceae	*Matteuccia struthiopteris*	5.2	0.071	59
Ophioglossaceae	*Botrychium lunaria*	1.6	0.035	59
Ophioglossaceae	*Botrychium ternatum*	4	0.05	57
Ophioglossaceae	*Ophioglossum vulgatum*	2	0.07	59
Osmundaceae	*Osmunda regalis*	8.5	0.077	59
Polypodiaceae	*Lepisorus thunbergianus*	8	0.04	57
Psilotaceae	*Psilotum nudum*	4	0.025	57
Pteridaceae	*Adiantum capillus-veneris*	5.9	0.059	59
Pteridaceae	*Adiantum pedatum*	2.8	0.04	59
Pteridaceae	*Athyrium filix-femina*	8.2	0.112	59
Pteridaceae	*Pteris vittata*	9.1	0.062	59
Thelypterdiaceae	*Thelypteris acuminata*	6.1	0.125	57
Thelypterdiaceae	*Thelypteris curta*	3.8	0.18	55
Thelypterdiaceae	*Thelypteris dentata*	6.3	0.144	59
Thelypterdiaceae	*Thelypteris palustris*	8.2	0.138	59

Extended Data Fig. 9 | See next page for caption.

Extended Data Fig 9 | Table of maximum photosynthetic gas exchange in diverse species. Maximum rates of gas exchange collected under standard conditions for species of lycophyte and ferns taken from the literature or measured in this study.

55. Campany, C. E., Martin, L. & Watkins, J. J. E. Convergence of ecophysiological traits drives floristic composition of early lineage vascular plants in a tropical forest floor. *Ann. Bot.* **123**, 793–803 (2019).
56. Soni, D. K. et al. Photosynthetic characteristics and the response of stomata to environmental determinants and ABA in *Selaginella bryopteris*, a resurrection spike moss species. *Plant Sci.* **191–192**, 43–52 (2012).
57. Doi, M., Kitagawa, Y. & Shimazaki, K.-i Stomatal blue light response is present in early vascular plants. *Plant Physiol.* **169**, 1205–1213 (2015).
58. Zier, J., Belanger, B., Trahan, G. & Watkins, J. E. Ecophysiology of four co-occurring lycophyte species: an investigation of functional convergence. *AoB Plants* **7**, plv137 (2015).
59. Tosens, T. et al. The photosynthetic capacity in 35 ferns and fern allies: mesophyll CO_2 diffusion as a key trait. *New Phytol.* **209**, 1576–1590 (2016).

nature research

Corresponding author(s): Timothy Brodribb

Last updated by author(s): 7/Jan/20

Reporting Summary

Nature Research wishes to improve the reproducibility of the work that we publish. This form provides structure for consistency and transparency in reporting. For further information on Nature Research policies, see Authors & Referees and the Editorial Policy Checklist.

Statistics

For all statistical analyses, confirm that the following items are present in the figure legend, table legend, main text, or Methods section.

n/a	Confirmed	
☐	☒	The exact sample size (*n*) for each experimental group/condition, given as a discrete number and unit of measurement
☐	☒	A statement on whether measurements were taken from distinct samples or whether the same sample was measured repeatedly
☐	☒	The statistical test(s) used AND whether they are one- or two-sided *Only common tests should be described solely by name; describe more complex techniques in the Methods section.*
☐	☒	A description of all covariates tested
☐	☒	A description of any assumptions or corrections, such as tests of normality and adjustment for multiple comparisons
☐	☒	A full description of the statistical parameters including central tendency (e.g. means) or other basic estimates (e.g. regression coefficient) AND variation (e.g. standard deviation) or associated estimates of uncertainty (e.g. confidence intervals)
☐	☒	For null hypothesis testing, the test statistic (e.g. *F*, *t*, *r*) with confidence intervals, effect sizes, degrees of freedom and *P* value noted *Give P values as exact values whenever suitable.*
☒	☐	For Bayesian analysis, information on the choice of priors and Markov chain Monte Carlo settings
☒	☐	For hierarchical and complex designs, identification of the appropriate level for tests and full reporting of outcomes
☒	☐	Estimates of effect sizes (e.g. Cohen's *d*, Pearson's *r*), indicating how they were calculated

Our web collection on statistics for biologists contains articles on many of the points above.

Software and code

Policy information about availability of computer code

Data collection	Image J (NIH, USA) was for collecting data from both SEM images and cavitation image sequences.
Data analysis	SigmaPlot (SPSS) was used to fit regressions. Spreadsheet software (MS Excel) was used to run model simulations. P

PyHST2 software (open source) was used for microCT reconstruction. ImageJ (opensource- National Institute of Health) was used for image sequence analysis.

Data

Policy information about availability of data

All manuscripts must include a data availability statement. This statement should provide the following information, where applicable:

- Accession codes, unique identifiers, or web links for publicly available datasets
- A list of figures that have associated raw data
- A description of any restrictions on data availability

All data generated or analysed during this study are included in this published article (and its supplementary information files).

Field-specific reporting

Please select the one below that is the best fit for your research. If you are not sure, read the appropriate sections before making your selection.

☒ Life sciences ☐ Behavioural & social sciences ☐ Ecological, evolutionary & environmental sciences

For a reference copy of the document with all sections, see nature.com/documents/nr-reporting-summary-flat.pdf

Life sciences study design

All studies must disclose on these points even when the disclosure is negative.

Sample size	Due to the high degree of relatedness in the individuals collected each measurement was considered as a replicate and a sample size of n=10 was considered sufficient to ensure strong replication of anatomical and hydraulic behaviour. Gas exchange measures were completed on larger sample sizes (50-100 individuals) to provide maximum resolution of dynamic responses.
Data exclusions	No data were excluded
Replication	Data were collected from a single species, hence the repeated measurements detailed in sample size constitute replicates. All replicates were successful
Randomization	Samples were not exposed to growth treatments, so randomization was not applied to sample selection. Individual selection was undertaken to minimize the size /age range among plants.
Blinding	No treatments were applied so no blinding was necessary.

Reporting for specific materials, systems and methods

We require information from authors about some types of materials, experimental systems and methods used in many studies. Here, indicate whether each material, system or method listed is relevant to your study. If you are not sure if a list item applies to your research, read the appropriate section before selecting a response.

Materials & experimental systems

n/a	Involved in the study
☒	☐ Antibodies
☒	☐ Eukaryotic cell lines
☒	☐ Palaeontology
☐	☒ Animals and other organisms
☒	☐ Human research participants
☒	☐ Clinical data

Methods

n/a	Involved in the study
☒	☐ ChIP-seq
☒	☐ Flow cytometry
☒	☐ MRI-based neuroimaging

Animals and other organisms

Policy information about studies involving animals; ARRIVE guidelines recommended for reporting animal research

Laboratory animals	no animals
Wild animals	no animals
Field-collected samples	Plants were maintained in a glasshouse under a natural photoperiod and illumination between 10 and 25°C. Misting was triggered every 20 minutes to ensure plants remained well-hydrated. Plants remained growing on their original substrate during the course of the experimental work
Ethics oversight	no animals

Note that full information on the approval of the study protocol must also be provided in the manuscript.